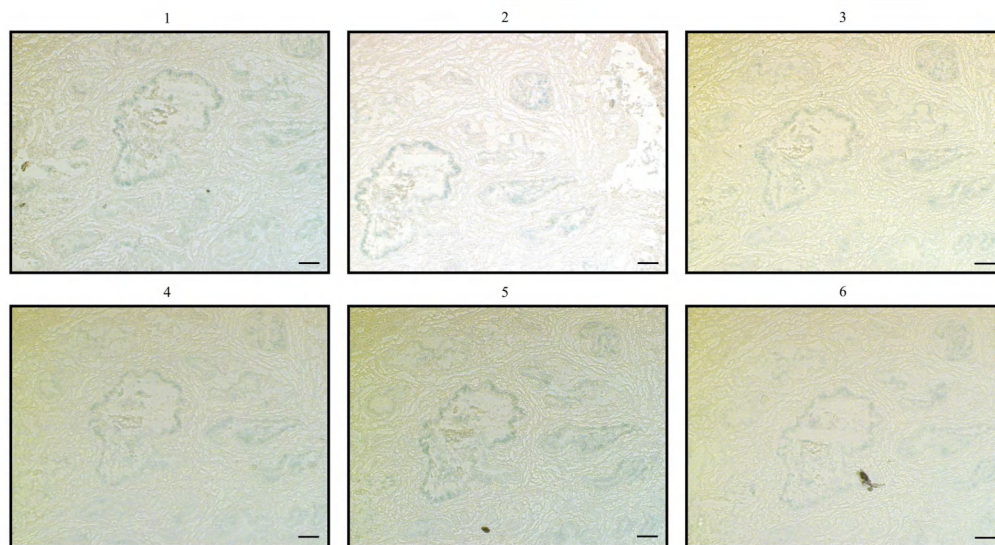
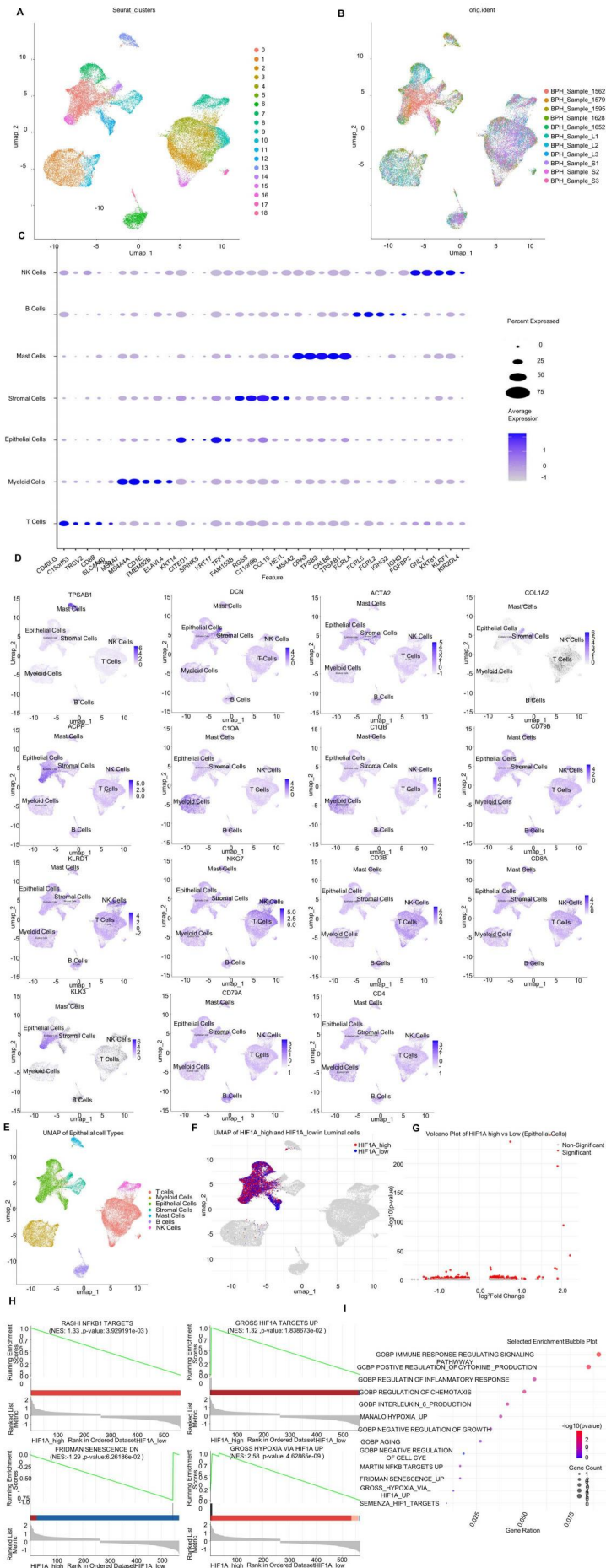


## Supplementary Figures



**Supplementary Figure S1. Serial-section SA-β-gal staining in BPH tissues.**

Serial frozen sections were used to assess the consistency of SA-β-gal staining within the same glandular structure. SA-β-gal staining was generally consistent within the same gland. Scale bar = 100 μm.



**Supplementary Figure S2. Single-cell transcriptomic analysis of prostate tissues from BPH patients.**

(A) UMAP plot displaying clusters identified using the Seurat algorithm, with each color representing a distinct cell type in the prostate transitional zone.

(B) UMAP plot showing cells color-coded by patient origin, highlighting inter-sample variability and integration across samples.

(C) Dot plot showing the expression of marker genes used to annotate major cell types, including *DCN*, *ACTA2*, and *COL1A2* for stromal cells; *KLK3* and *ACPP* for epithelial cells; *CIQA* and *CIQB* for myeloid cells; *CD79A* and *CD79B* for B cells; *KLRD1* and *NKG7* for NK cells; and *CD3D*, *CD4*, and *CD8A* for T cells.

(D) Feature plots of representative marker-gene expression confirming the identity of each cell lineage in the UMAP visualization.

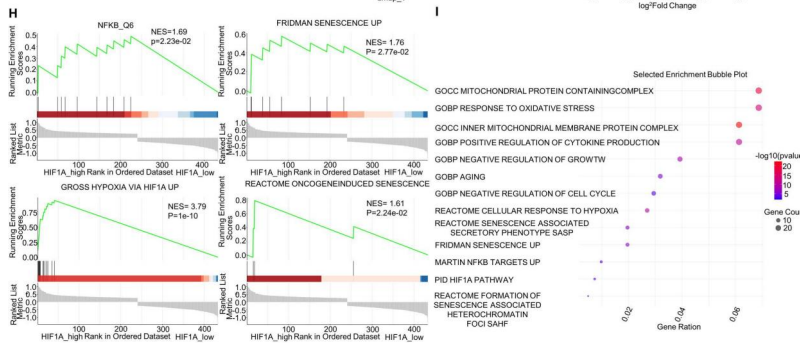
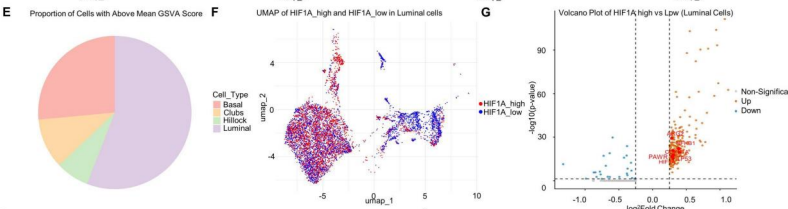
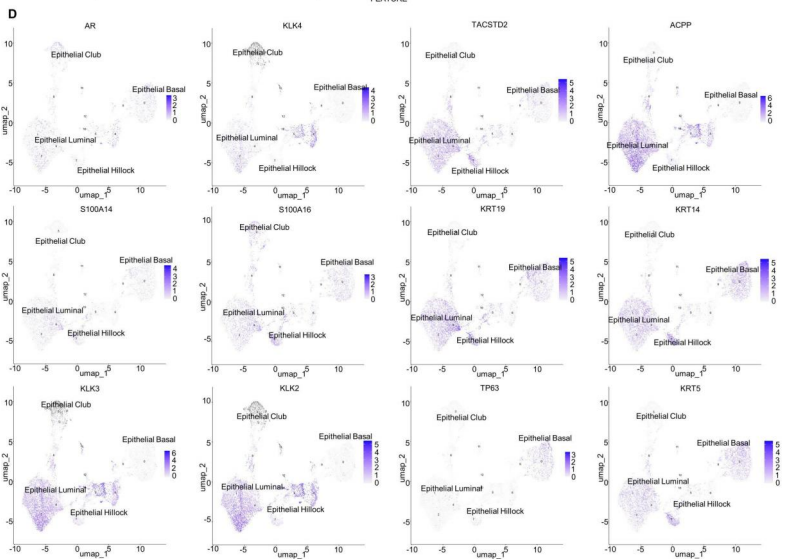
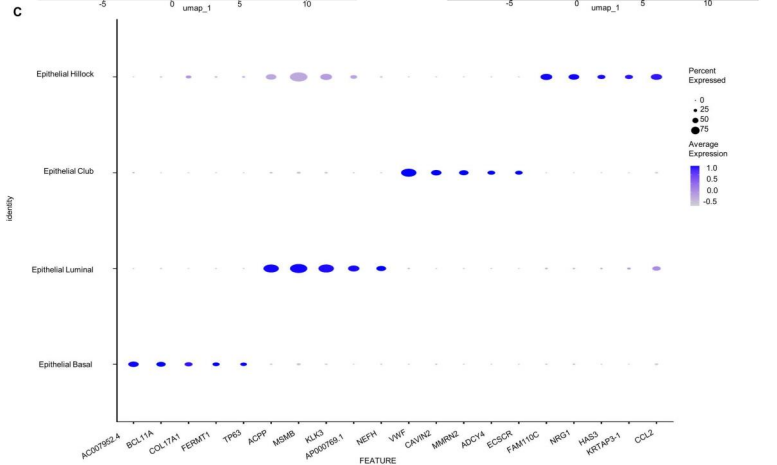
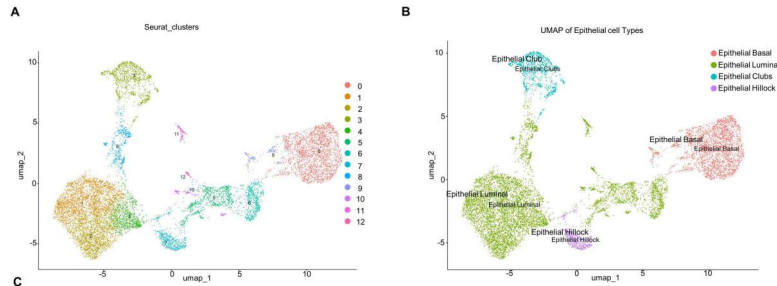
(E) UMAP projection of the six major cell types identified in the human BPH scRNA-seq dataset, including T cells, myeloid cells, epithelial cells, stromal cells, NK cells, and B cells.

(F) UMAP projection of epithelial cells stratified into HIF-1 $\alpha$  pathway-high and HIF-1 $\alpha$  pathway-low groups based on GSVA scores for the MSigDB gene set GROSS\_HYPOXIA\_VIA\_HIF1A\_UP, highlighting the enrichment of Luminal cells in the HIF-1 $\alpha$  pathway-high group.

(G) Volcano plot showing DEGs between HIF-1 $\alpha$  pathway-high and HIF-1 $\alpha$  pathway-low epithelial cells. Red dots indicate significantly upregulated genes, and blue dots indicate significantly downregulated genes.

(H) GSEA plots showing pathways enriched in HIF-1 $\alpha$  pathway-high epithelial cells, including hypoxia-related pathways and NF- $\kappa$ B signaling.

(I) Bubble plot analysis of hypoxia- and senescence-related pathways significantly enriched in HIF-1 $\alpha$  pathway-high epithelial cells.



**Supplementary Figure S3. Detailed analysis of epithelial cells in the transitional zone of prostate tissues from BPH patients.**

(A) UMAP plot showing clustering of 10,727 epithelial cells from BPH prostate tissues, classified into four epithelial subtypes: Luminal, Basal, Hillock, and Club cells.

(B) Dot plot showing the expression of key marker genes distinguishing the four epithelial subtypes.

(C) UMAP plot of epithelial subtypes.

(D) Feature plots showing the expression patterns of key marker genes across epithelial subtypes, including *AR*, *KLK4*, *TACSTD2*, *ACPP*, *S100A14*, *S100A16*, and *KRT19*.

(E) Pie chart showing the proportion of epithelial subtypes with above-mean GSVA scores for the hypoxia/HIF-1 $\alpha$ -related signature.

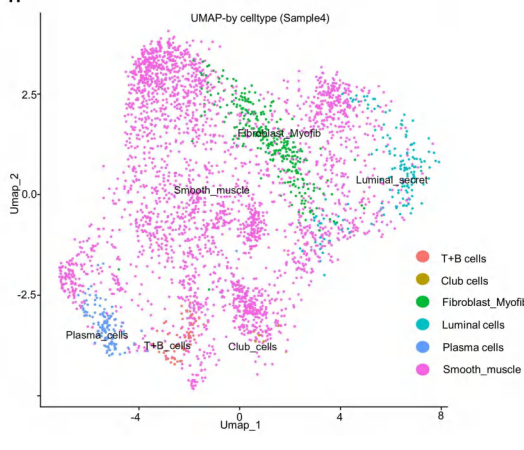
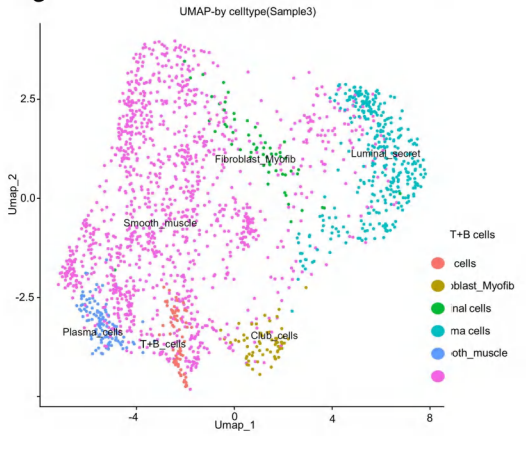
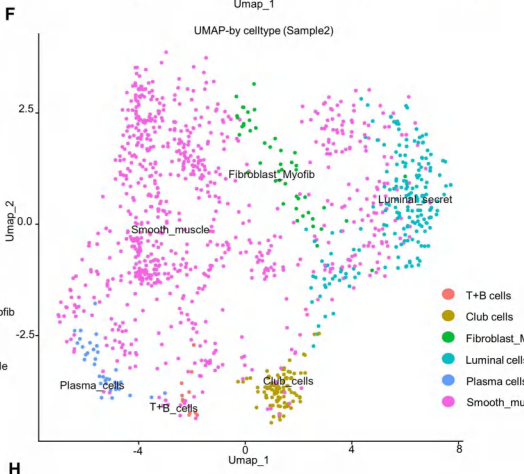
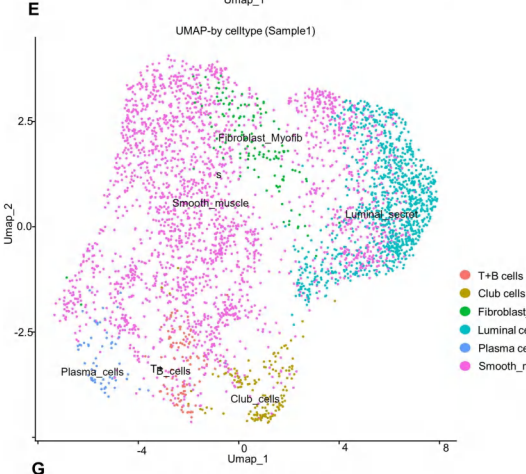
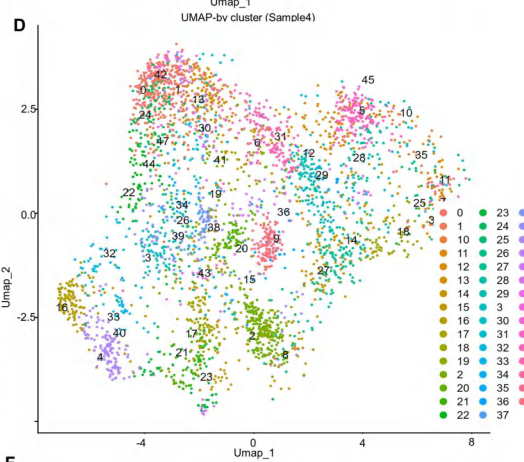
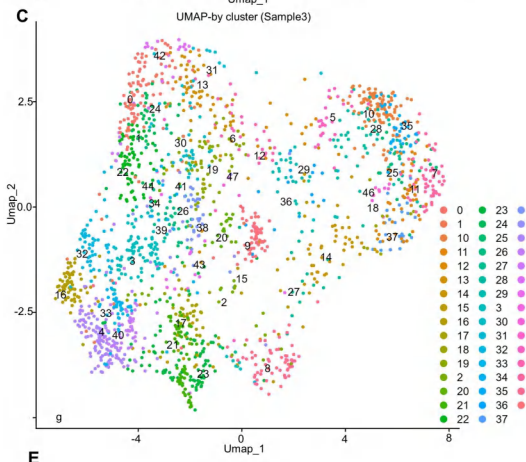
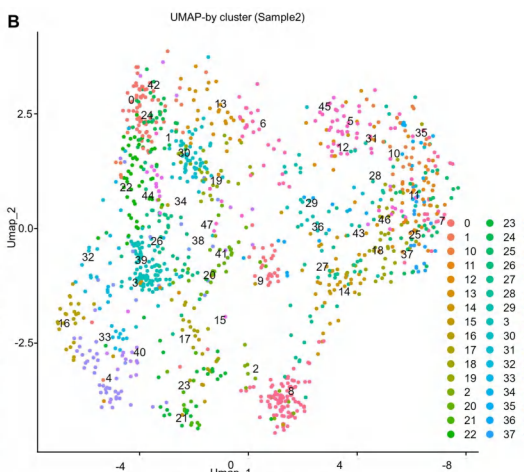
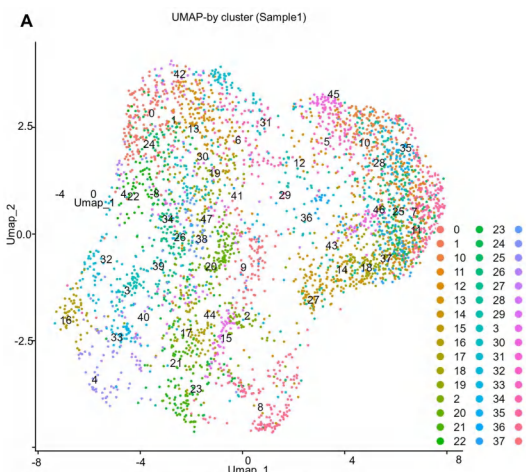
(F) UMAP projection of epithelial cells stratified into HIF-1 $\alpha$  pathway-high and HIF-1 $\alpha$  pathway-low groups based on GSVA scores for the MSigDB gene set GROSS\_HYPOXIA\_VIA\_HIF1A\_UP, highlighting the predominance of Luminal cells in the HIF-1 $\alpha$  pathway-high group.

(G) Volcano plot showing DEGs between HIF-1 $\alpha$  pathway-high and HIF-1 $\alpha$  pathway-low epithelial cells. Representative senescence-associated and pathway-related genes selected for cross-dataset comparison, including *ARG2*, *PAWR*, *TP53*, *HIF1A*, *NFKB1*, and *CDKN1A*, are labeled.

(H) GSEA plots showing significant enrichment of hypoxia-, NF- $\kappa$ B-, and senescence-related pathways, including NFKB\_Q6, FRIDMAN\_SENESCENCE\_UP, GROSS\_HYPOXIA\_VIA\_HIF1A\_UP, and REACTOME\_ONCOGENE\_INDUCED\_SENESCENCE.

(I) Selected enrichment bubble plot showing gene ratio and statistical significance of

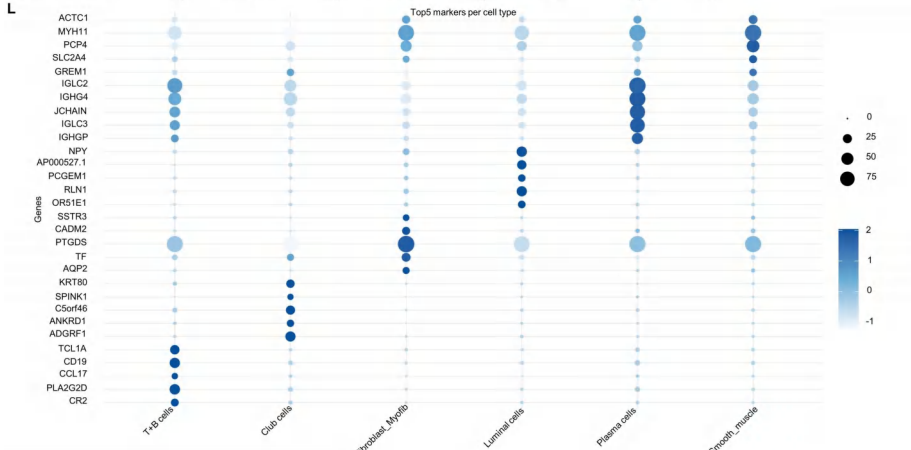
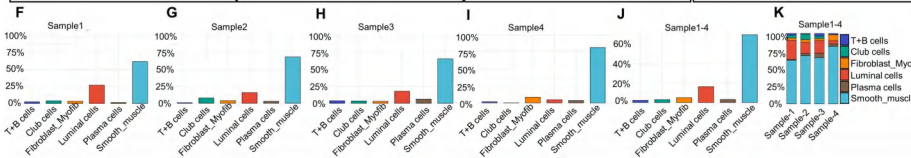
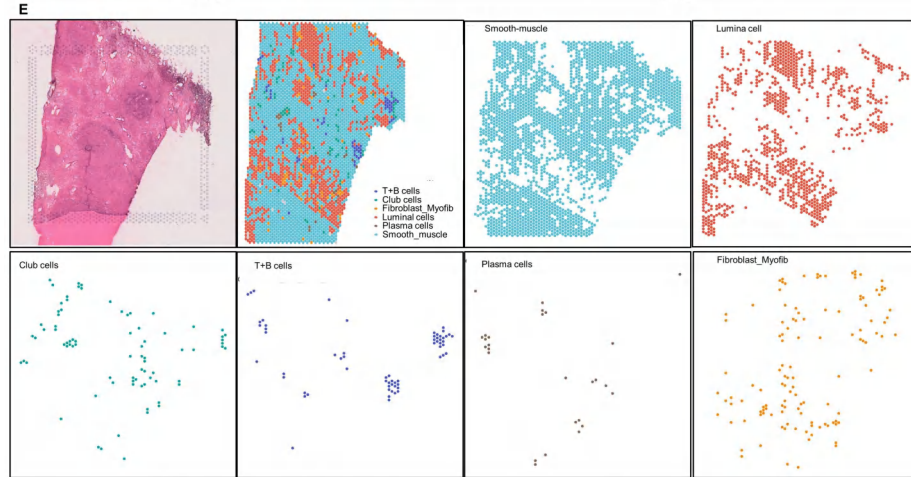
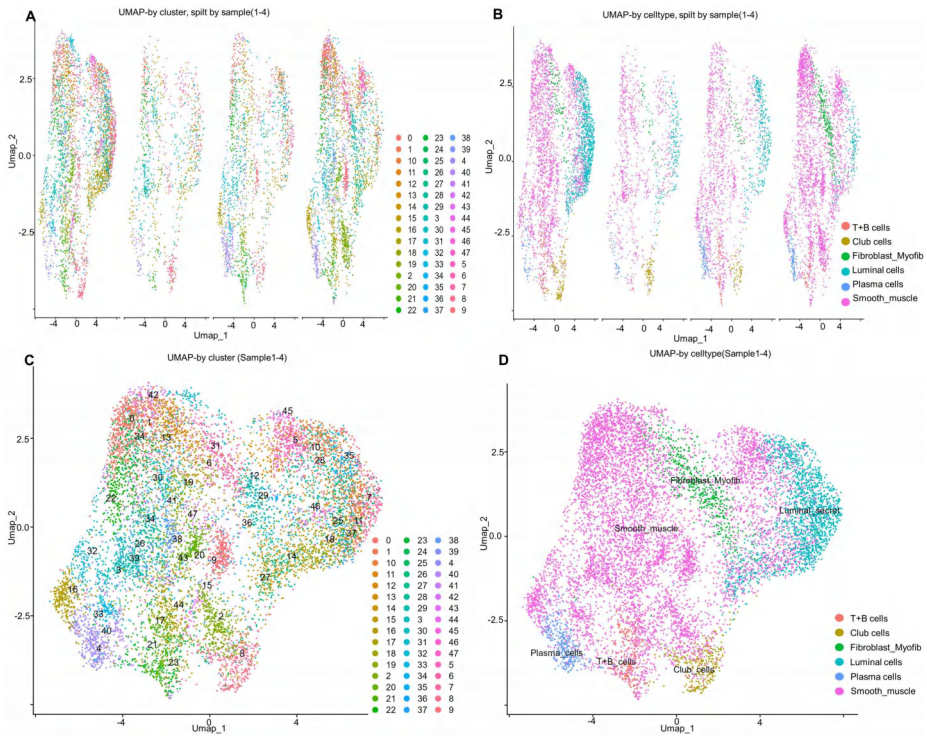
pathways related to mitochondrial function, oxidative stress, cytokine production, growth regulation, and senescence in epithelial cell subtypes.



**Supplementary Figure S4. Sample-wise spatial transcriptomic analysis and reference-based spot annotation of BPH tissues.**

(A–D) UMAP embeddings of spatial transcriptomic spots from four BPH samples, analyzed separately to illustrate sample-level transcriptomic heterogeneity before cross-sample integration.

(E–H) Reference-based annotation of spatial spots following label transfer from the scRNA-seq reference, identifying six major dominant spot identities or cell states: Smooth\_muscle cells, Luminal cells, Fibroblast\_Myofib cells, Plasma cells, Club cells, and T+B cells.



**Supplementary Figure S5. Integrated spatial transcriptomic atlas and compositional features of BPH tissues.**

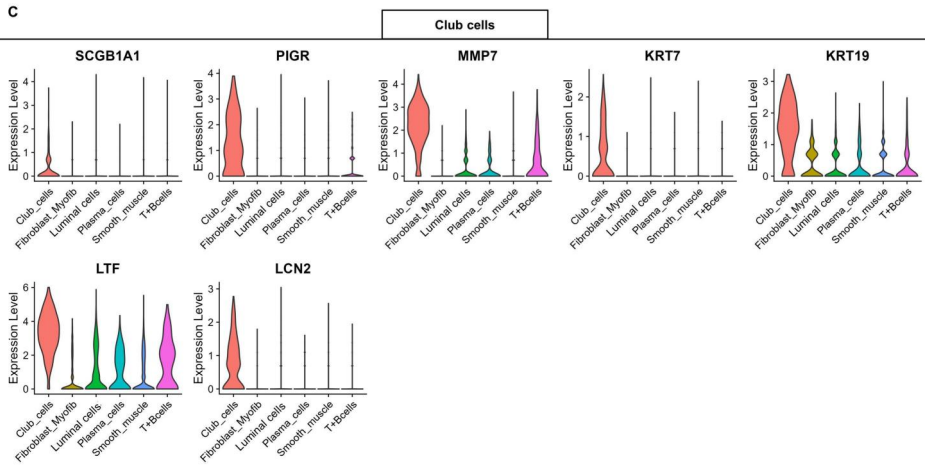
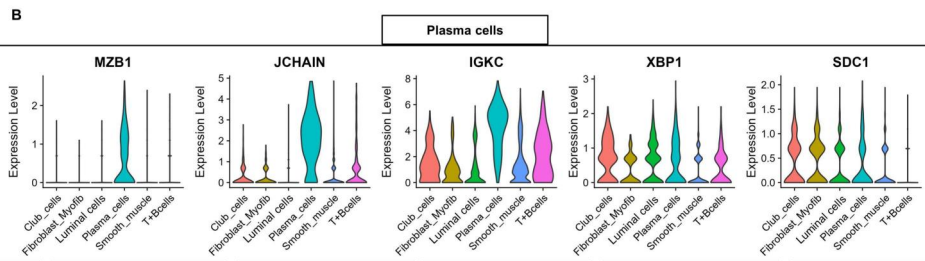
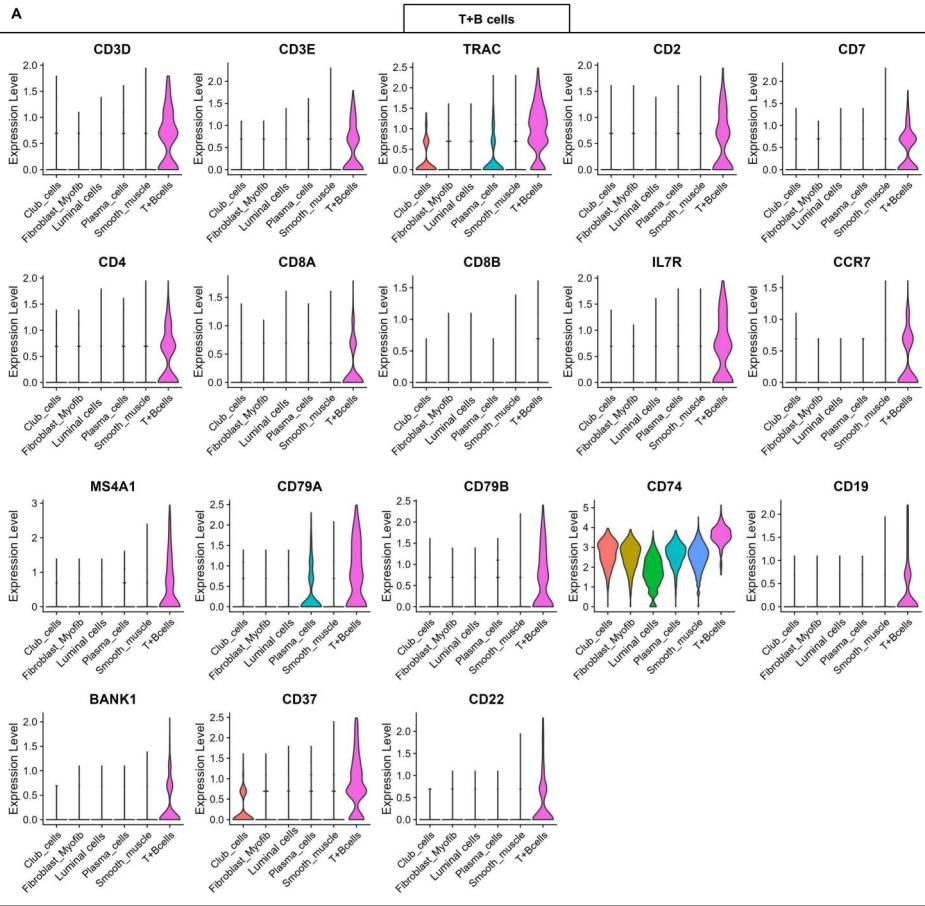
(A–D) Integrated UMAP plots of spatial transcriptomic spots from all four BPH samples, colored by sample origin (A, B) and by transferred dominant spot identity/cell state (C, D), showing effective cross-sample integration.

(E) Representative H&E-stained tissue section overlaid with transferred spot annotations, illustrating the spatial distribution of major lineages/cell states in BPH tissue.

(F–I) Proportions of major transferred spot identities/cell states in each individual spatial transcriptomic sample.

(J–K) Overall composition of transferred spot identities/cell states across all four samples, shown as a bar plot (J) and stacked bar plot (K).

(L) Supportive summary of selected marker-gene expression patterns across major transferred spatial spot identities/cell states. Detailed marker-expression validation for individual annotated populations is shown in Figs. S6–S7.

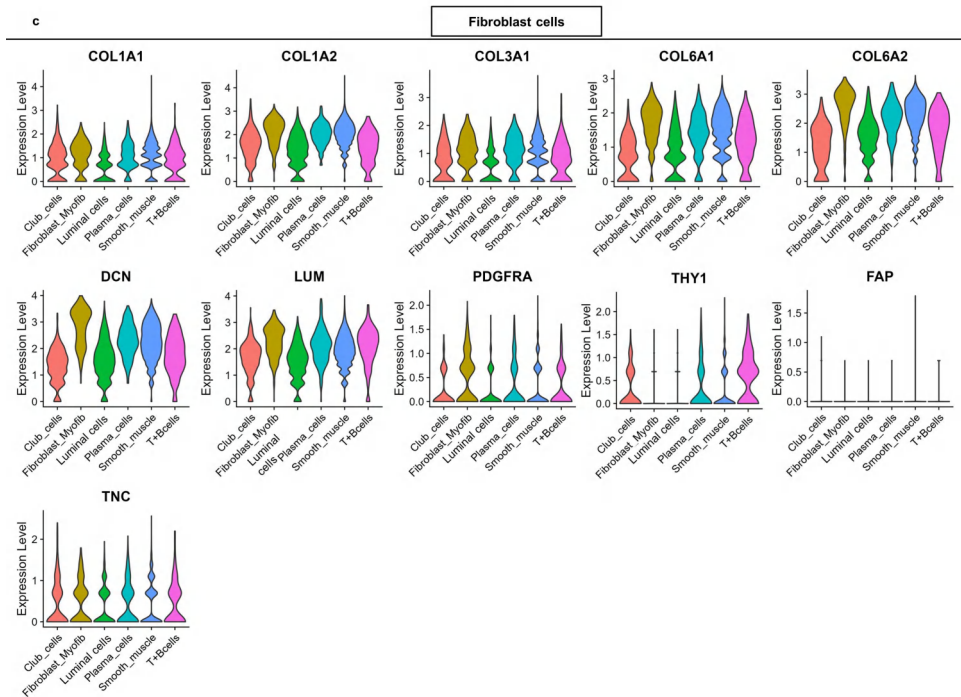
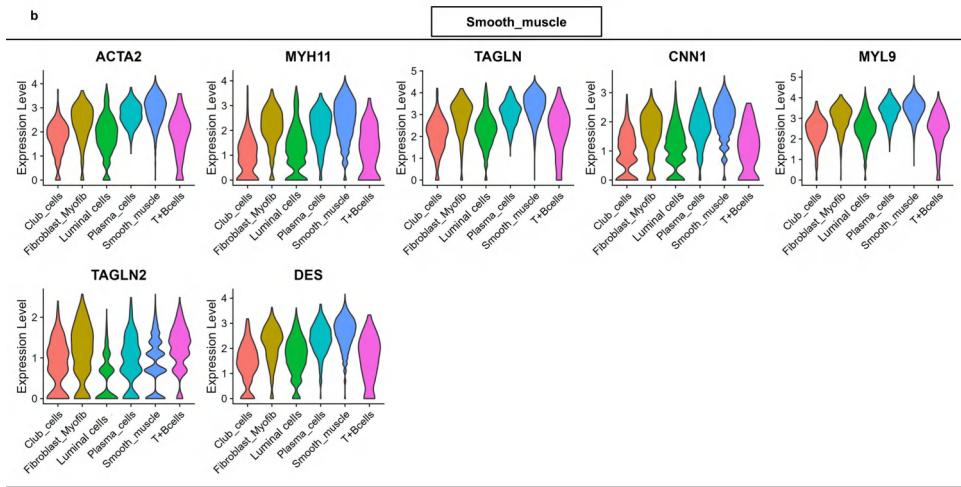
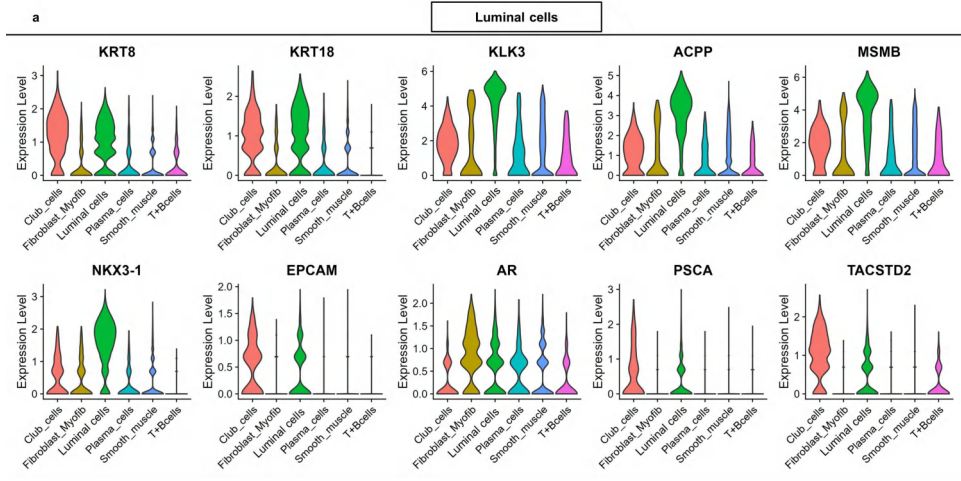


**Supplementary Figure S6. Representative marker-gene expression in T+B, Plasma, and Club cell populations.**

(A) Violin plots showing expression of canonical T- and B-cell markers in the T+B cell cluster, including *CD3D* and *CD4* as T-cell markers and *CD19* as a B-cell marker.

(B) Violin plots showing expression of plasma cell markers *MZB1*, *JCHAIN*, and *IGKC*, highlighting their selective enrichment in the Plasma cell population.

(C) Violin plots showing expression of representative Club cell markers *SCGB1A1*, *PIGR*, and *KRT7*, demonstrating their preferential expression in Club cells relative to other lineages.

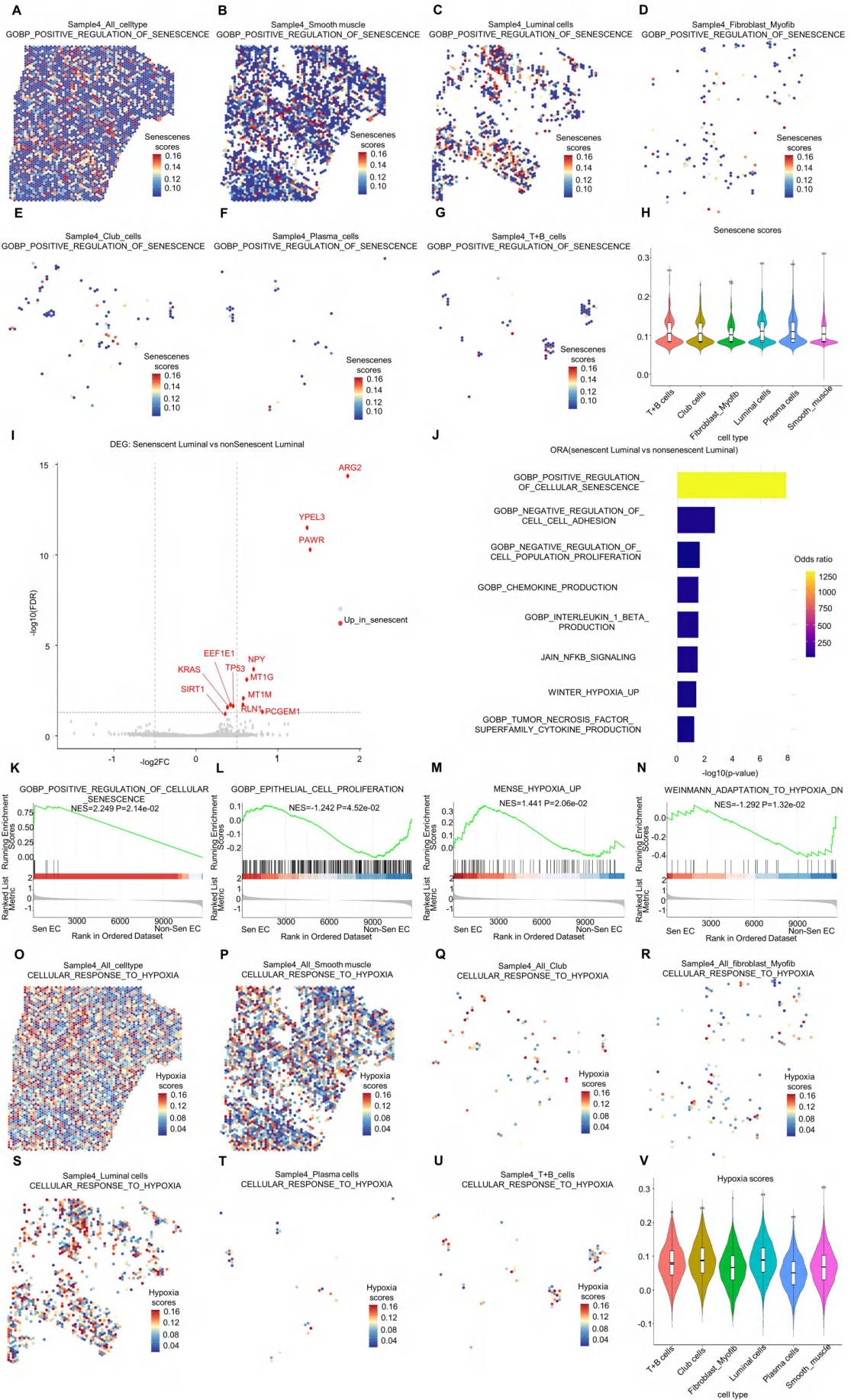


**Supplementary Figure S7. Representative marker-gene expression in Luminal, Smooth\_muscle, and Fibroblast\_Myofib populations.**

(A) Violin plots showing expression of luminal epithelial markers *KRT8*, *KLK3*, and *ACPP* in the Luminal cell population.

(B) Violin plots showing expression of smooth muscle markers *ACTA2*, *MYH11*, and *TAGLN* in the Smooth\_muscle population.

(C) Violin plots showing expression of fibroblast/myofibroblast-associated markers *COL1A1*, *DCN*, and *PDGFRA* in the Fibroblast\_Myofib population.



**Supplementary Figure S8. Spatial transcriptomic analysis of senescence- and hypoxia-associated transcriptional programs in human BPH prostate tissues.**

(A–G) Spatial feature maps showing UCell scores for GOBP\_POSITIVE\_REGULATION\_OF\_CELLULAR\_SENESCENCE across all spots and major transferred spot identities/cell states in representative spatial transcriptomic sections. The color scale indicates senescence-associated transcriptional scores.

(H) Violin plots with embedded boxplots showing senescence-associated UCell scores across major transferred spot identities/cell states. The embedded boxplots indicate the median and interquartile range. Luminal-dominant spots showed relatively high senescence-associated transcriptional scores compared with other major spot identities/cell states.

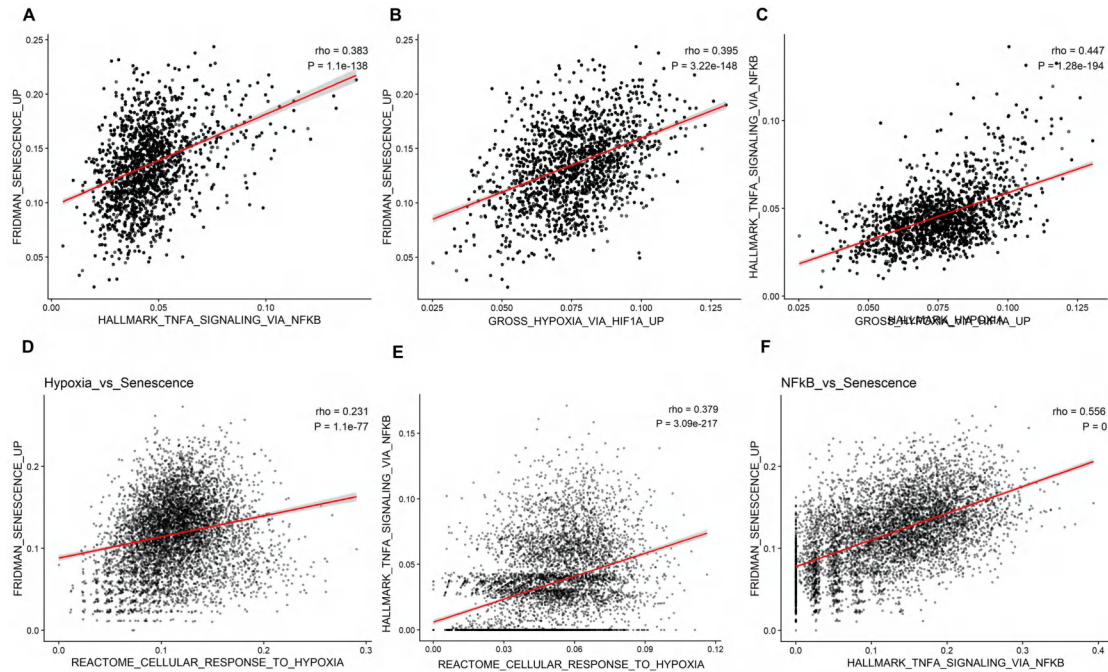
(I) Volcano plot showing differentially expressed genes between senescence-score-high and senescence-score-low Luminal-dominant spots. Representative upregulated genes in senescence-score-high Luminal-dominant spots, including ARG2, YPEL3, PAWR, KRAS, EEF1E1, and TP53, are labeled.

(J) Over-representation analysis of genes upregulated in senescence-score-high Luminal-dominant spots, showing enrichment of senescence-, inflammatory cytokine-, NF- $\kappa$ B-, and hypoxia-related biological processes or pathways.

(K–N) Gene set enrichment analysis of ranked genes comparing senescence-score-high and senescence-score-low Luminal-dominant spots. Senescence-associated and hypoxia-related signatures were positively enriched in senescence-score-high Luminal-dominant spots, whereas epithelial-cell proliferation and hypoxia-adaptation-down signatures showed negative enrichment.

(O–U) Spatial feature maps showing UCell scores for REACTOME\_CELLULAR\_RESPONSE\_TO\_HYPOXIA across all spots and major transferred spot identities/cell states in representative spatial transcriptomic sections. The color scale indicates hypoxia-response scores.

(V) Violin plots with embedded boxplots showing hypoxia-response UCell scores across major transferred spot identities/cell states. The embedded boxplots indicate the median and interquartile range.

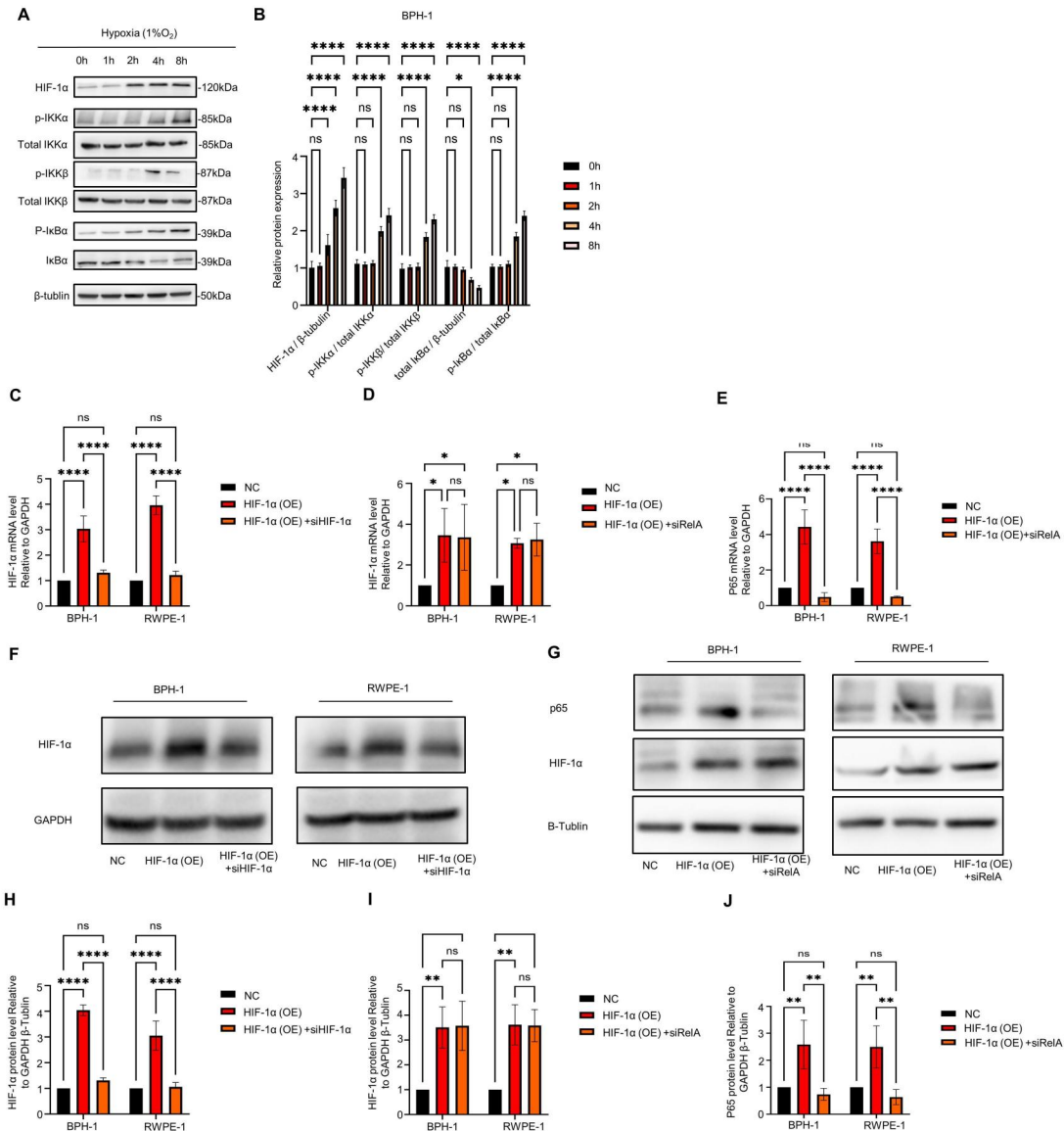


**Supplementary Figure S9. Correlation analysis of hypoxia-, NF- $\kappa$ B-, and senescence-associated pathway scores in single-cell and spatial transcriptomic datasets.**

(A–C) Scatter plots showing pairwise correlations among pathway scores in epithelial cells from the human BPH scRNA-seq dataset. Pathway activity was scored using gene sets applied in the single-cell analysis, including GROSS\_HYPOXIA\_VIA\_HIF1A\_UP for hypoxia/HIF-1 $\alpha$  pathway activity, HALLMARK\_TNFA\_SIGNALING\_VIA\_NFKB for NF- $\kappa$ B-related inflammatory signaling, and FRIDMAN\_SENESCENCE\_UP for cellular senescence. Positive correlations were observed between NF- $\kappa$ B and senescence scores (A), hypoxia/HIF-1 $\alpha$  and senescence scores (B), and hypoxia/HIF-1 $\alpha$  and NF- $\kappa$ B scores (C).

(D–F) Scatter plots showing pairwise correlations among pathway scores in spatial

transcriptomic spots from human BPH tissues. Spatial pathway activity was scored using `REACTOME_CELLULAR_RESPONSE_TO_HYPOXIA` for hypoxia response, `HALLMARK_TNFA_SIGNALING_VIA_NFKB` for NF- $\kappa$ B signaling, and `GOBP_POSITIVE_REGULATION_OF_CELLULAR_SENESCENCE` for senescence-associated transcriptional activity. Positive correlations were observed between hypoxia and senescence scores (D), hypoxia and NF- $\kappa$ B scores (E), and NF- $\kappa$ B and senescence scores (F). Red lines indicate fitted linear trends. Correlations were assessed using Spearman's rank correlation analysis; rho and P values are shown in each panel. For the spatial dataset, pathway scores represent spot-level transcriptional activity and should not be interpreted as single-cell state assignments.



**Supplementary Figure S10. Time-course analysis of HIF-1 $\alpha$  accumulation and IKK/I $\kappa$ B $\alpha$  phosphorylation under hypoxia and validation of HIF-1 $\alpha$ /RELA genetic manipulation efficiency.**

(A) Western blot analysis of HIF-1 $\alpha$ , p-IKK $\alpha$ , total IKK $\alpha$ , p-IKK $\beta$ , total IKK $\beta$ , p-I $\kappa$ B $\alpha$ , total I $\kappa$ B $\alpha$ , and  $\beta$ -tubulin in BPH-1 cells exposed to 1% O<sub>2</sub> hypoxia for the indicated time points. Groups 1–5 represent 0, 1, 2, 4, and 8 h of hypoxia exposure, respectively.

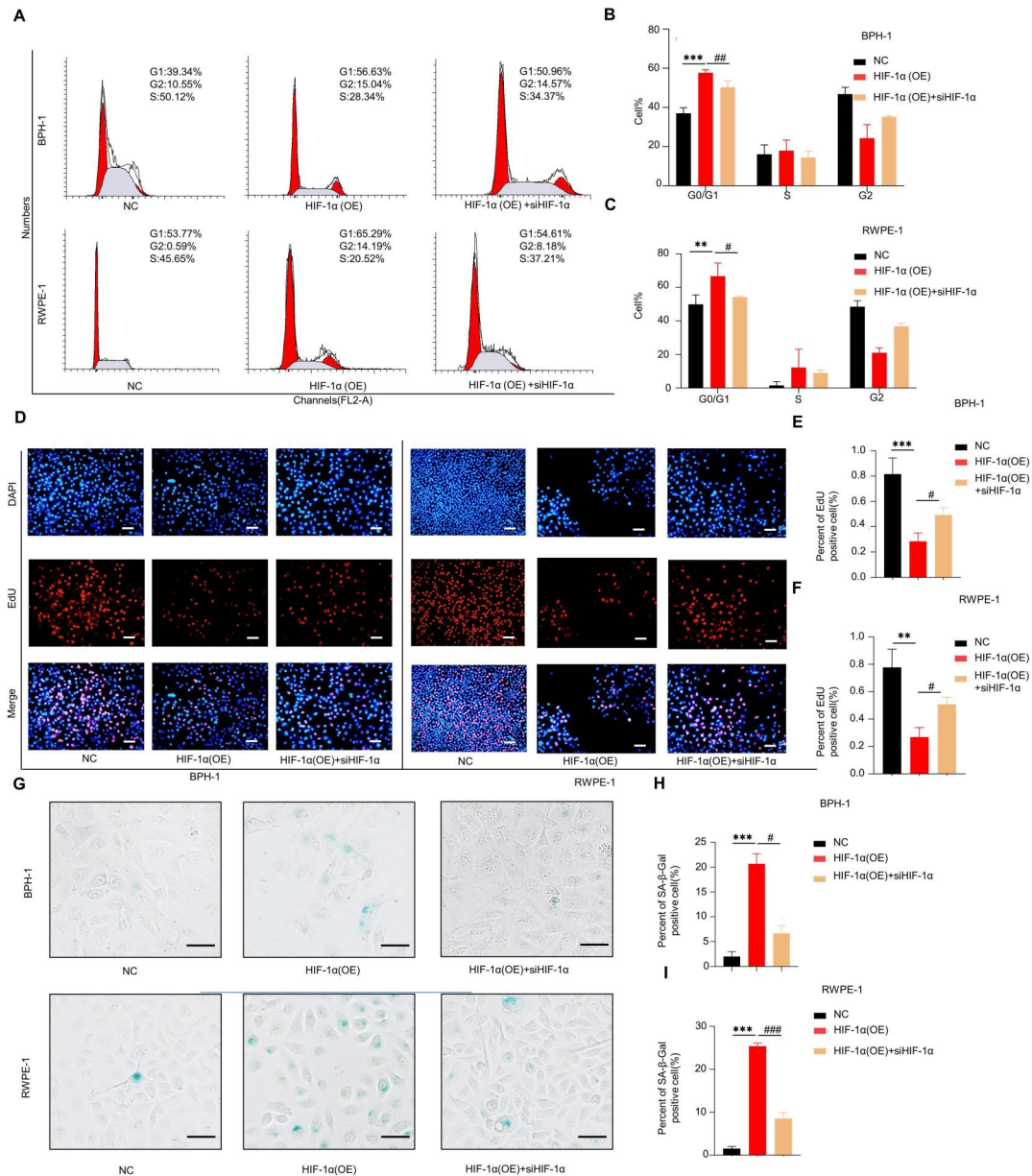
(B) Quantification of the indicated proteins in (A). HIF-1 $\alpha$  and total I $\kappa$ B $\alpha$  were normalized to  $\beta$ -tubulin. p-IKK $\alpha$ , p-IKK $\beta$ , and p-I $\kappa$ B $\alpha$  were normalized to total IKK $\alpha$ , total IKK $\beta$ , and total I $\kappa$ B $\alpha$ , respectively. All values were expressed relative to group 1.

(C) qRT-PCR analysis of *HIF1A* mRNA levels in BPH-1 and RWPE-1 cells after HIF-1 $\alpha$  overexpression with or without si*HIF1A* co-transfection.

(D, E) qRT-PCR analysis of *HIF1A* (D) and *RELA* (E) mRNA levels in BPH-1 and RWPE-1 cells after HIF-1 $\alpha$  overexpression with or without si*RELA* co-transfection.

(F, H) Western blot analysis (F) and quantification (H) of HIF-1 $\alpha$  protein levels in BPH-1 and RWPE-1 cells after HIF-1 $\alpha$  overexpression with or without si*HIF1A* co-transfection. GAPDH was used as the loading control.

(G, I, J) Western blot analysis (G) and quantification of HIF-1 $\alpha$  (I) and p65 (J) protein levels in BPH-1 and RWPE-1 cells after HIF-1 $\alpha$  overexpression with or without si*RELA* co-transfection.  $\beta$ -tubulin was used as the loading control. Data are presented as the mean  $\pm$  SD. ns, not significant;  $P < 0.05$ ;  $P < 0.01$ ;  $P < 0.001$ ;  $P < 0.0001$ .

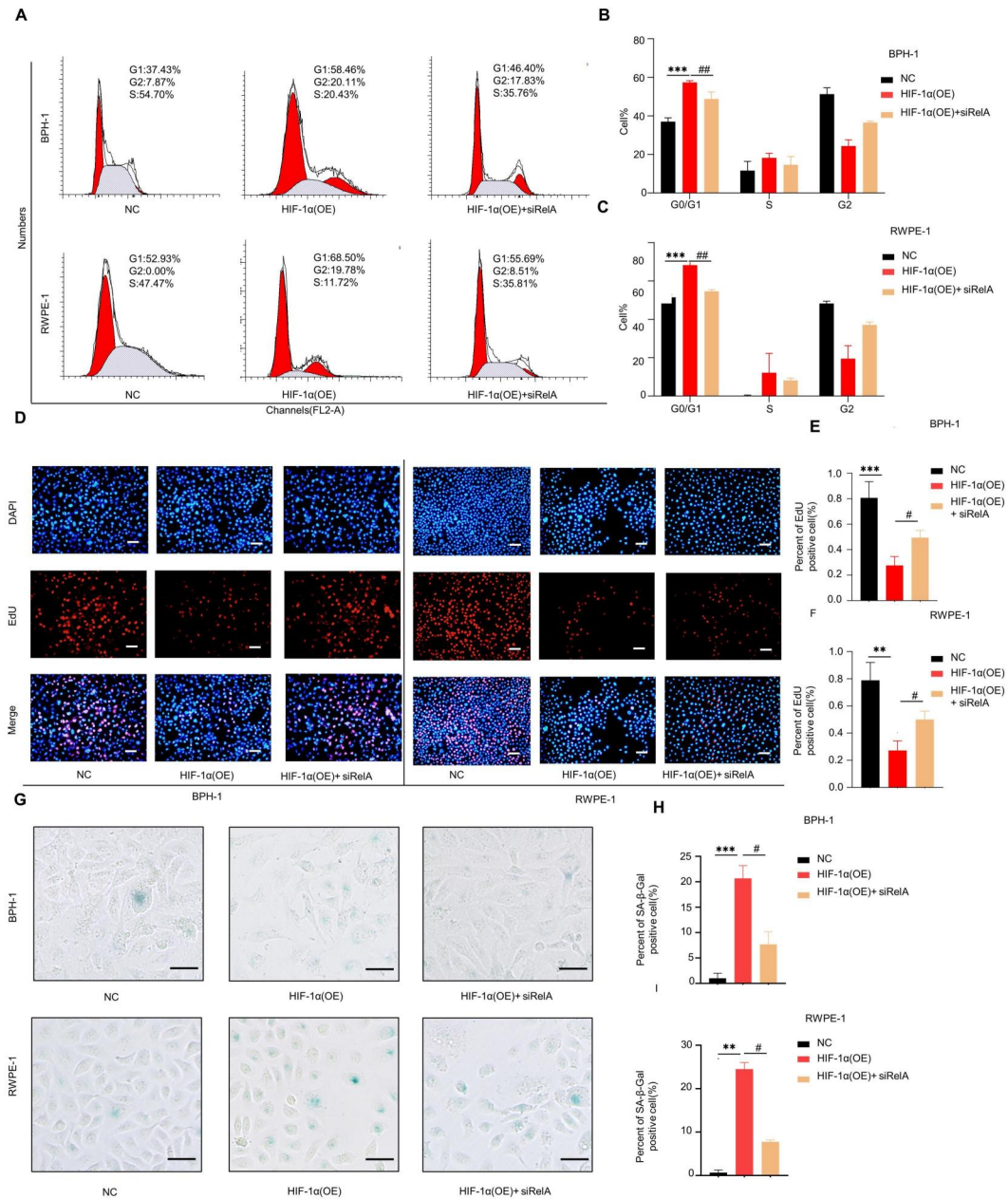


**Supplementary Figure S11. HIF-1α overexpression induces senescence-associated phenotypes in prostate epithelial cells.**

(A–C) Flow cytometric analysis showing the cell-cycle distribution of BPH-1 and RWPE-1 cells in the control, HIF-1α overexpression, and HIF-1α overexpression + siHIF1A groups.

(D–F) EdU assays showing the proliferation of BPH-1 and RWPE-1 cells in the control, HIF-1α overexpression, and HIF-1α overexpression + siHIF1A groups. Scale bar = 100 μm.

(G-I) SA- $\beta$ -gal staining of BPH-1 and RWPE-1 cells in the control, HIF-1 $\alpha$  overexpression, and HIF-1 $\alpha$  overexpression + siHIF1A groups. Scale bar = 100  $\mu$ m. All data are presented as the mean  $\pm$  standard deviation, n = 3. \*P < 0.05, \*\*P < 0.01, \*\*\*P < 0.001; #P < 0.05, ##P < 0.01, ###P < 0.001.



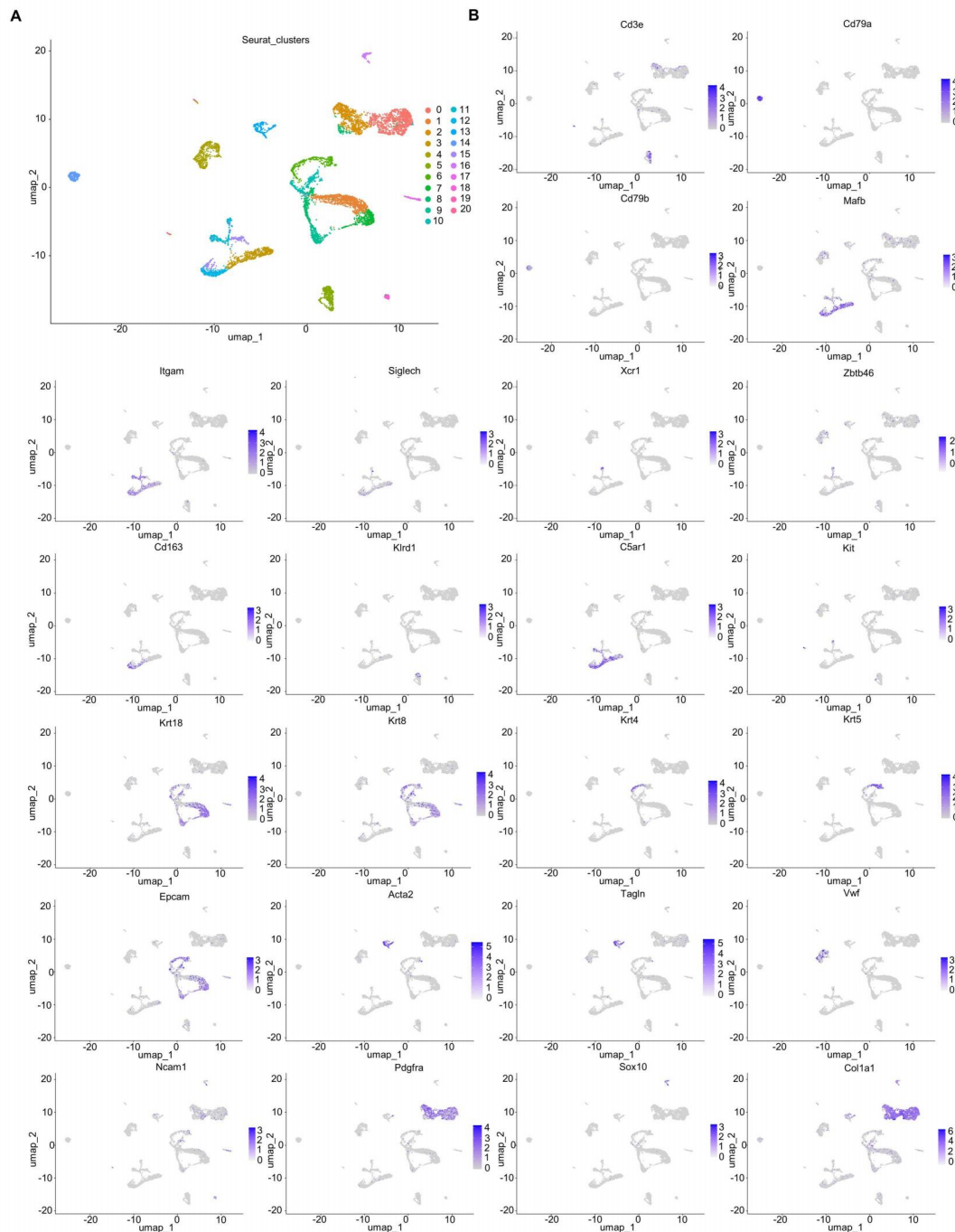
**Supplementary Figure S12. NF- $\kappa$ B signaling contributes to HIF-1 $\alpha$ -induced senescence-associated phenotypes in prostate epithelial cells.**

(A–C) Flow cytometric analysis showing the cell-cycle distribution of BPH-1 and RWPE-1 cells in the control, HIF-1 $\alpha$  overexpression, and HIF-1 $\alpha$  overexpression + si*RELA* groups.

(D–F) EdU assays showing the proliferation of BPH-1 and RWPE-1 cells in the control, HIF-1 $\alpha$  overexpression, and HIF-1 $\alpha$  overexpression + si*RELA* groups. Scale bar = 100  $\mu$ m.

(G–I) SA- $\beta$ -gal staining of BPH-1 and RWPE-1 cells in the control, HIF-1 $\alpha$  overexpression, and HIF-1 $\alpha$  overexpression + si*RELA* groups. Scale bar = 100  $\mu$ m.

All data are presented as the mean  $\pm$  standard deviation, n = 3. \*P < 0.05, \*\*P < 0.01, \*\*\*P < 0.001; #P < 0.05, ##P < 0.01.

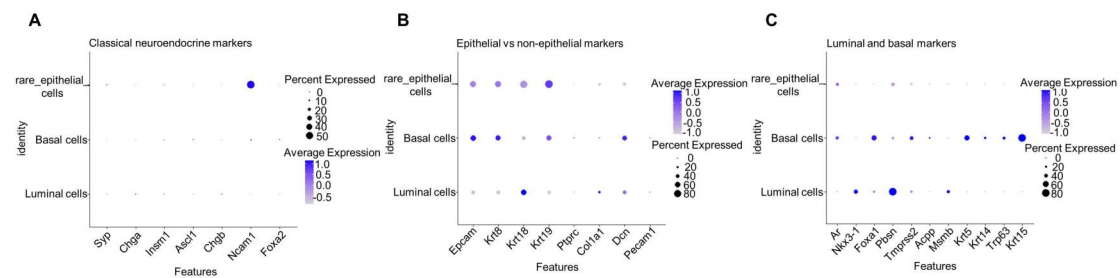


**Supplementary Figure S13. Single-cell transcriptomic atlas of castration plus testosterone-induced BPH in ICR male mice.**

(A) UMAP plot showing 7,316 cells classified into nine major cell lineages based on marker-gene expression. The identified cell types include T/NK cells, B cells, myeloid cells, epithelial cells, mast cells, myofibroblasts, fibroblasts, smooth muscle cells, and endothelial cells.

(B) Feature plots of representative marker genes used to define each cell type,

including *Il2rb* and *Nkg7* for T/NK cells, *Cd19* and *Pax5* for B cells, *Mpeg1* and *Clec4a2* for myeloid cells, *Krt18* and *Krt8* for epithelial cells, *Cma1* and *Tpsab1* for mast cells, *Acta2* and *Pdgfra* for myofibroblasts, *Colla1* for fibroblasts, *Rgs5* and *Actg2* for smooth muscle cells, and *Cdh5* and *Sox18* for endothelial cells. Expression intensity is shown on a blue gradient, with darker shades indicating higher expression levels.

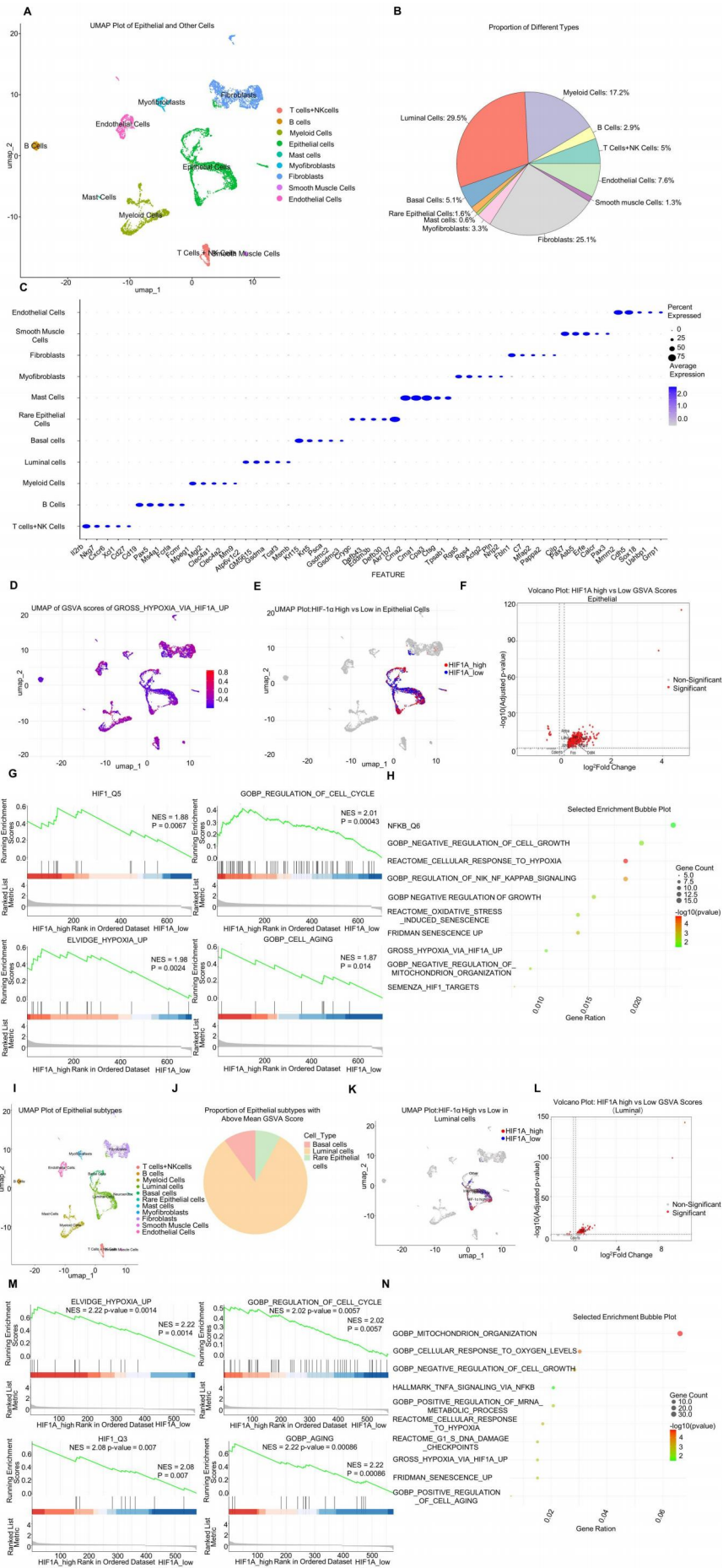


**Supplementary Figure S14. Marker-based support for reannotation of the minor epithelial cluster as rare epithelial cells in the mouse prostate scRNA-seq dataset.**

(A) Dot plot showing expression of classical neuroendocrine markers, including *Syp*, *Chga*, *Insm1*, *Ascl1*, *Chgb*, *Ncam1*, and *Foxa2*, across luminal, basal, and rare epithelial cell populations. The rare epithelial cluster does not show a coherent canonical neuroendocrine marker program.

(B) Dot plot comparing epithelial and non-epithelial markers across luminal, basal, and rare epithelial cell populations. Rare epithelial cells retain epithelial-marker expression, including *Epcam*, *Krt8*, *Krt18*, and *Krt19*, and do not show clear enrichment of non-epithelial markers such as *Ptprc*, *Colla1*, *Dcn*, and *Pecam1*.

(C) Dot plot showing representative luminal and basal markers across epithelial subtypes. Rare epithelial cells do not fully conform to either the canonical luminal program, represented by *Ar*, *Nkx3-1*, *Pbsn*, *Tmprss2*, *Acpp*, and *Msmb*, or the basal program, represented by *Krt5*, *Krt14*, *Trp63*, and *Krt15*. These findings support their conservative annotation as a distinct rare epithelial population.



**Supplementary Figure S15. Single-cell RNA sequencing reveals hypoxia-, NF- $\kappa$ B-, and senescence-associated transcriptional programs in castration plus testosterone-induced BPH.**

(A) UMAP plot showing the distribution of epithelial and non-epithelial cell types identified in castration plus testosterone-induced BPH. Cells were classified into T/NK cells, B cells, myeloid cells, epithelial cells, mast cells, myofibroblasts, fibroblasts, smooth muscle cells, and endothelial cells.

(B) Pie chart showing the proportions of identified cell types. Epithelial cells accounted for the largest proportion, including Luminal cells, Basal cells, and rare epithelial cells, followed by fibroblasts, myeloid cells, and smaller contributions from other cell types.

(C) Dot plot showing expression of representative marker genes across the nine cell lineages. Immune-related markers such as *Il2rb* and *Nkg7* were enriched in T/NK cells, whereas *Cd19* and *Pax5* marked B cells. *Mpeg1* and *Clec4a2* highlighted myeloid cells, and epithelial markers such as *Krt18*, *Krt8*, and *Krt5* revealed heterogeneity within the epithelial compartment. Stromal markers such as *Colla1* and vascular markers such as *Cdh5* confirmed the identities of fibroblasts and endothelial cells, respectively. Additional marker-expression analyses supporting the reannotation of rare epithelial cells are shown in Fig. S14A–C.

(D) UMAP plot showing GSVA scores for the GROSS\_HYPOXIA\_VIA\_HIF1A\_UP gene set across different cell types, with prominent hypoxia pathway activation observed in epithelial and stromal cells.

(E) UMAP plot of epithelial cells stratified into HIF-1 $\alpha$  pathway-high and HIF-1 $\alpha$  pathway-low groups based on GSVA scores.

(F) Volcano plot showing DEGs between HIF-1 $\alpha$  pathway-high and HIF-1 $\alpha$  pathway-low epithelial cells. Representative genes related to hypoxia/HIF signaling, NF- $\kappa$ B-associated inflammatory responses, and senescence/cell-cycle regulation are highlighted, including *Aldoa*, *Pgk1*, *Ldha*, *Ddit4*, *Nfkb1a*, *Cdkn1b*, *Jun*, *Junb*, and *Fos*.

(G) GSEA plots showing pathways enriched in HIF-1 $\alpha$  pathway-high epithelial cells.

Representative enriched pathways include ELVIDGE\_HYPOXIA\_UP, GOBP\_REGULATION\_OF\_CELL\_CYCLE, and GOBP\_CELL\_AGING, reflecting hypoxia adaptation, cell-cycle regulation, and aging-associated transcriptional programs.

(H) Bubble plot of enriched pathways in HIF-1 $\alpha$  pathway-high epithelial cells, highlighting REACTOME\_CELLULAR\_RESPONSE\_TO\_HYPOXIA, FRIDMAN\_SENESCENCE\_UP, and HALLMARK\_TNFA\_SIGNALING\_VIA\_NFKB.

(I) UMAP projection of epithelial subtypes identified in the mouse prostate scRNA-seq dataset, including Luminal cells, Basal cells, and rare epithelial cells.

(J) Pie chart showing the proportion of epithelial subtypes with above-mean GSVA scores for the GROSS\_HYPOXIA\_VIA\_HIF1A\_UP pathway. Luminal cells comprised the majority, reflecting their dominant contribution to hypoxia-associated pathway activity in the epithelial compartment.

(K) UMAP plot of Luminal cells stratified into HIF-1 $\alpha$  pathway-high and HIF-1 $\alpha$  pathway-low groups based on GSVA scores.

(L) Volcano plot showing DEGs between HIF-1 $\alpha$  pathway-high and HIF-1 $\alpha$  pathway-low Luminal cells, highlighting representative significant genes, including *Cdkn1b* and *Ddit4*.

(M) GSEA plots for Luminal cells, showing enrichment of hypoxia-responsive pathways, including ELVIDGE\_HYPOXIA\_UP; cell-cycle regulation, including GOBP\_REGULATION\_OF\_CELL\_CYCLE; and aging-related processes, including GOBP\_AGING.

(N) Bubble plot of enriched pathways in HIF-1 $\alpha$  pathway-high Luminal cells, highlighting hypoxia response, represented by REACTOME\_CELLULAR\_RESPONSE\_TO\_HYPOXIA; NF- $\kappa$ B signaling, represented by HALLMARK\_TNFA\_SIGNALING\_VIA\_NFKB; and senescence, represented by FRIDMAN\_SENESCENCE\_UP.